Potential-Induced Wetting and Dewetting in pH-Responsive Block Copolymer Membranes for Mass Transport Control

Seung-Ryong Kwon[1†], Seol Baek[2†], and Paul W. Bohn[2,3*]

[1]Department of Chemistry and Research Institute of Natural Science, Gyeongsang National University, Jinju, 52828, South Korea

[2]Department of Chemistry and Biochemistry, University of Notre Dame, Notre Dame, Indiana 46556, United States

[3]Department of Chemical and Biomolecular Engineering, University of Notre Dame, Notre Dame, Indiana 46556, United States

[†]Seung-Ryong Kwon and Seol Baek contributed equally to this work.

[*]Author to whom correspondence should be addressed, pbohn@nd.edu

Abstract

Wetting and dewetting behavior in channel-confined hydrophobic volumes is used in biological membranes to effect selective ion/molecular transport. Artificial biomimetic hydrophobic nanopores have been devised utilizing wetting and dewetting, however, tunable mass transport control utilizing multiple transport modes is required for applications such as controllable release/transport, water separation/purification, and energy conversion. Here, we investigate potential-induced wetting and dewetting behavior in a pH-responsive membrane composed of polystyrene-*b*-poly(4-vinylpyridine) (PS-*b*-P4VP) block copolymer (BCP) when fabricated as a hierarchically-organized sandwich structure on a nanopore electrode array (NEA), *i.e.* BCP@NEA. At pH < pK_a(P4VP) (pK_a ~ 4.8), the BCP acts as an anion-exchange membrane due to the hydrophilic, protonated P4VP cylindrical nanodomains, but at pH > pK_a(P4VP), the P4VP domains exhibit charge-neutral, hydrophobic, and collapsed structures, blocking mass transport *via* the hydrophobic membrane. However, when originally prepared in a dewetted condition, mass transport in the BCP membrane may be switched on if sufficiently negative potentials are applied to the BCP@NEA architecture. When the hydrophobic BCP membrane is introduced on top of 2-electrode-embedded nanopore arrays, electrolyte solution in the nanopores is introduced, then isolated, by exploiting potential-induced wetting and dewetting transitions in the BCP membrane. The potential-induced wetting/dewetting transitions and their effect on cyclic voltammetry in the BCP@NEA structures is characterized as a function of potential, pH, and ionic strength. In addition, chronoamperometry and redox cycling experiments are used to further characterize the potential response. The multi-modal mass transport system proposed in this work will be useful for ultrasensitive sensing and single-molecule studies, which require long-time monitoring to explore reaction dynamics as well as molecular heterogeneity in nanoconfined volumes.

Introduction

Living organisms achieve selective ion/molecular transport by using actively-controlled protein channels in cell membranes, a function which serves many biological functions such as the transmission of nerve signals, muscle contraction, and substance transport.[1,2] In biological channels such as nicotinic acetylcholine receptor channels, potassium, and magnesium channels, a hydrophobic cavity in the channel pathway plays a key role in selectively transporting ions or molecules, exhibiting fast gating action.[3-5] The flux of ions/molecules with co-permeating water is regulated by the wettability of the hydrophobic domain in the channel, which is reversibly switched between wetted and dewetted states in response to an external stimulus, such as a concentration gradient or an electric field. Not surprisingly and motivated by these characteristics, great effort has been expended on preparing artificial biomimetic nanopores for applications to water purification/collection, biochemical sensing and smart valves for controlled release and delivery.[6-12]

The use of wettability switching controlled by an external stimulus, *e.g.,* electric field, light, pH, and pressure, to produce repeatable high and low ionic currents in hydrophobic nanopores has attracted significant interest. For example, Smirnov and co-workers investigated wetting and dewetting behavior in hydrophobic nanopores controlled by light,[13] pH,[14] pressure,[15] and voltage.[16] They demonstrated reversible switching of wettability in hydrophobic nanopores controlled by an electric field and demonstrated a 1000-fold difference in conductance between wetted (high conductivity) and dewetted (low conductivity) states.[16] Siwy and co-workers further developed this concept by employing single hydrophobic nanopores with high aspect ratios - 12 μm-long conically shaped pore with a 16 nm-diameter opening - achieving on/off switching (non-conducting and conducting ionic current) based on electric-field-induced reversible wetting and dewetting.[17] Jiang and co-workers realized dual-

stimuli-, *i.e.*, electrostatic-charge- and electric-field-, responsive wetting and dewetting behaviors using surface-charged nanochannels,[18] and more recently reported light- and electric-field-controlled wetting behavior in functionalized conical polymer nanopores by adapting a light-responsive host-guest reaction.[19]

Our laboratory has long been interested in mass transport behavior in confined geometries composed of nanoscale pores. Electrochemical transistors were demonstrated in 3-electrode embedded nanopore electrode arrays (NEAs) based on potential-controlled wetting and dewetting inside defect-mediated nanochannels.[20] Furthermore, surface charge on the nanopore wall has been shown to exhibit a significant effect on ion accumulation and exclusion at low ionic strength. Exploiting this effect, a ~2000-fold current amplification was achieved.[21] In addition, ion-selective electrochemical detection was realized by tailoring the surface charge in nanopores.[22] Recently, hierarchically organized membrane-coated NEAs have been devised using either Nafion or polystyrene-*b*-poly-4-vinylpyridine (PS-*b*-P4VP) to achieve cation- and anion-selectivity, respectively. Coupling these block copolymer (BCP) structures to NEAs (BCP@NEA) enables the current amplification characteristics of the NEA to be combined with the pH-dependent ion-permselectivity of the BCP membranes.[23, 24]

To date however, regulation of mass transport by integrating inputs from multiple control signals has not been realized. In the regards the PS-*b*-P4VP BCP@NEA structure is of interest, because the PS-*b*-P4VP membrane exhibits pH-dependent mass transport behavior above and below the pK_a of the P4VP block (pK_a ~ 4.8). At pH < pK_a, the P4VP cylindrical domains are protonated at the pyridine nitrogen atom, rendering them swollen and hydrophilic, and consequently the BCP membrane acts as an anion-exchange membrane. In contrast, at pH > pK_a, the P4VP domains exhibit charge-neutral, hydrophobic, and collapsed structures. Thus, inspired by the previous mass transport control in hydrophobic nanopores, here we report the

systematic investigation of potential-induced wetting and dewetting behavior of BCP@NEA structures as a function of pH, membrane thickness, and ionic strength to achieve a mass transport system with a multi-modal control paradigm. As shown in **Figure 1**, the BCP@NEA architectures exhibit: (1) anion-selective transport at pH < pK_a(P4VP), and at pH > pK_a(P4VP) (2*a*) no transport in the absence of external potential, and (2*b*) strong, charge-independent ion transport upon switching the P4PV nanochannels to the wetted state at sufficiently negative potentials. These characteristics of the BCP membrane make it possible to reversibly confine solution in nanopores and to isolate it from bulk solution. The multi-modal mass transport system developed in this work holds potential for ultrasensitive sensors as well as single molecule studies, which requires long-time monitoring of reaction dynamics.

Results and Discussion

Mass transport in PS-b-P4VP BCP membranes vs. pH. In order to study mass transport behavior in the pH-responsive PS-*b*-P4VP membrane, a BCP membrane was prepared by spin-coating 2% (w/v) PS-*b*-P4VP in dioxane onto a planar Au electrode at 6000 rpm for 1 min, producing an 81 nm thick membrane, as shown in the SEM image in **Figure 2(a)** *inset*. BCP membranes were characterized electrochemically at different pH values. First, a pH 8.4 solution containing 5 mM $Fe(CN)_6^{3-}$ in 0.1 M KCl was used to render the P4VP domains charge-neutral, collapsed, and hydrophobic. The hydrophobic BCP membranes obtained at pH > pK_a(P4VP) blocks mass transport of aqueous solutions. This behavior has previously been observed and assigned to evaporation of water being more favorable in the hydrophobic P4VP nanochannels than the condensation of water.[10, 25]

Cyclic voltammetry was performed to investigate the effect of an external potential on the mass transport through the BCP membrane. At pH 8.4 > pK_a(P4VP), no current response is

observed in the potential range from +0.5 V > E_{appl} > –0.4 V *vs*. Ag/AgCl, where a Nernstian response would be expected from $Fe(CN)_6^{3/4-}$, but a rapid increase in current is observed at $E_{appl} \leq$ –0.4 V, **Figure 2(a)**. It should be noted that electrochemical hysteresis is observed in the voltammograms, especially in the first potential scan (see **Supporting Information**, **Figure S1** showing voltammograms of the first potential cycle). A rapid increase in cathodic current is observed in the negative-going scan starting at $E_{appl} \sim$ –0.85 V. Given that the resting state of the BCP membrane at this pH is hydrophobic and dewetted, the observation of current indicates conversion of the hydrophobic P4VP membrane channels to a wetted state, in which the condensation of water dominates over evaporation. In addition, the currents in **Figure 2(a)** display hysteresis, with the current on the return positive-going scan being larger than the negative-going current at the same potential. This suggests that once the hydrophobic P4VP membrane channels are filled with electrolyte solution, they tend to maintain the wetted state. Upon reaching E_{appl} > –0.4 V, the P4VP channels recover the original dewetted state, as shown by the negligible current at –0.4 V < E_{appl} < 0.5 V in the return scan. Furthermore, increasing limiting currents are obtained with successive scans, suggesting that more membrane channels are involved in the potential-dependent wetting and dewetting responses with successive scans. Together, the two distinct electrochemical responses, *i.e.,* (*a*) no current response in the potential range +0.5 V > E_{appl} > –0.4 V, and (*b*) increasing current response with electrochemical hysteresis in the potential range between –0.4 V > E_{appl} > –1.0 V, suggest the primary role for potential-dependent wetting and dewetting in the hydrophobic BCP membrane at pH 8.4.

The behavior of the same BCP membrane was also characterized at pH 3.0, *i.e.*, pH < pK_a(P4VP). It has previously been shown that under these conditions, the P4VP nanodomains of the BCP membrane are hydrophilic and protonated exhibiting approximately cylindrical

structures. Under these conditions, a reversible current response of $Fe(CN)_6^{3/4-}$ is obtained, as expected from the anion-selective character of the BCP membrane at pH < pK_a(P4VP), **Figure 2(b)**. Notably, the cathodic peak current obtained at pH 3.0 is somewhat larger than the maximum current at pH 8.4 upon electric-field-induced wetting (*viz*. –45 and –65 μA at pH 8.4 and 3.0, respectively), implying that the sum total of the mass transport pathways under potential-induced wetting at pH 8.4 is less than those presented by the fully wetted P4VP domains at pH 3.0.

Cation transport through hydrophobic BCP membranes. Since the pH-responsive PS-*b*-P4VP functions as an anion-exchange membrane at pH < pK_a(P4VP), cyclic voltammetry was conducted with a positively charged redox species, *i.e.,* $Ru(NH_3)_6^{3+}$, to explore the charge-dependence of mass transport at pH > pK_a(P4VP) in the presence of an applied potential in order to define the conditions at which the hydrophobic BCP membrane switches to a wetted state. Thus, 5 mM $Ru(NH_3)_6^{3+}$ in 0.1 M KCl solution at pH 7.8 was characterized on two different thickness BCP membranes on planar Au electrodes to probe the effects of charge selectivity and membrane thickness. On a 160 nm thick BCP membrane, gradually increasing current responses are observed at negative potentials with increasing scan numbers, reaching quasi-steady state at *ca.* the 7th potential scan, **Figure 3(a)**. Electrochemical hysteresis was observed, similar to the experiments with $Fe(CN)_6^{3-}$, consistent with the potential-induced wetting interpretation. In contrast, an 89 nm thick BCP membrane produced a response which reaches a maximum after only 2 potential cycles, **Figure 3(b)**. Notably, the maximum current on the 89 nm membrane was *ca*. 2-fold higher than on the 160 nm membrane, reflecting the enhanced transport characteristics of the thinner BCP membrane. The key observation is that even though PS-*b*-P4VP BCP membranes are anion-permselective at pH < pK_a(P4VP), positively charged $Ru(NH_3)_6^{3+}$ is readily transported through the membrane at E_{appl} < –0.4 V,

thus confirming that potential-induced wetting transitions in the BCP membrane are independent of the charge of the test species.

Ionic strength-dependence of wetting/dewetting in BCP membranes. Potential-induced wetting and dewetting were also examined as a function of ionic strength (I) in the range 0.006 M < I < 1 M, corresponding to 0 - 1 M supporting electrolyte (SE), *i.e.,* KNO_3, with 1 mM $K_3[Fe(CN)_6]$ at pH 8.4. Interestingly, a negligible voltammetric response was obtained from 1 mM $Fe(CN)_6^{3-}$ in the absence of SE over the potential range, $-1.0\ V \leq E_{appl} \leq +0.5\ V$, used for previous measurements, **Figure 4(a)** red curve. However, extending the negative potential limit to −1.2 V produces electrochemical behavior similar to the observed in **Figure 2(a)**, *i.e.,* scan-dependent limiting currents and electrochemical hysteresis, consistent with wetting/dewetting. The BCP membrane behavior was subsequently characterized in a pH 3.1 electrolyte solution containing the same concentration of redox species, *i.e.*, 1 mM $Fe(CN)_6^{3-}$ without SE. As shown in **Figure S2**, current gradually increased with scan number, and quasi-reversible voltametric responses centered at the formal potential of $Fe(CN)_6^{3-}$ were obtained. The gradual recovery of the $Fe(CN)_6^{3/4-}$ current is consistent with regaining anion-selectivity with the protonated pyridine in P4VP nanocylinders and demonstrates the mechanical and chemical stability of the BCP membranes to changing potentials, pH, and ionic strength conditions.

Next, the concentration of the supporting electrolyte was increased from 10 mM to 1000 mM. At 10 mM SE, as shown in **Figure 4(b)**, the BCP membrane exhibits potential-induced electrowetting over a narrower potential range, only requiring −1.0 V to induce transport. Once again, gradually increasing current is observed with accumulating scan numbers, and a steady-state current response is obtained after 7 potential cycles. When the SE concentration is further increased to 100 mM only 3 potential cycles are required to reach the maximum current value at −1.0 V, **Figure 4(c)**, and at 1000 mM SE, the maximum SE concentration used in these

experiments, potential-induced wetting is further promoted, such that only -0.8V is needed to induced enhanced currents, **Figure 4(d)**. These experiments clearly demonstrate that it is easier to induce transport across the BCP membrane at high ionic strength and suggests that the underlying electrowetting transitions are facilitated under these conditions.

Isolation of electrolyte solution in nanopores. Having demonstrated the ability to control transport across the PS-*b*-P4VP membrane with external potential as well as pH, we next constructed architectures combining the BCP membrane with NEAs, *i.e.* BCP@NEAs. These structures were built to test the ability to isolate and confine an electrolyte solution apart from the bulk solution using potential-controlled wetting and dewetting of PS-*b*-P4VP BCPs. NEAs were fabricated using a combination of nanosphere lithography and reactive ion etching applied to multilamellar metal-insulator-metal-insulator (MIMI, from bottom to top) structures. BCP membranes were transferred from Si substrates onto NEAs using thermal release tape, as shown in **Figure S3**. Transferring the membrane onto the NEA produced no apparent damage, **Figure S3(b)**, and cross-sectional SEM images revealed good attachment of the membrane on the outer surface of the NEA with well-preserved nanopore structures, **Figures S3(c)** and **(d)**. It should be noted that rather thick ~1.2 μm BCP membranes were required to maintain physical integrity with the NEA structures. However, these thicker membranes proved competent to control mass transport *via* potential-induced wetting and dewetting, as shown below. Moreover, these MIMI structures were terminated with a 500 nm top SiO_2 layer to facilitate capture of aqueous solution as well as to reduce the influence of the membrane hydrophobicity on electrochemical response.

When the BCP@NEA device was exposed to 50 mM $Fe(CN)_6^{3/4-}$ without SE at pH 7.6 in the absence of an applied potential, mass transport through the hydrophobic BCP membrane was blocked as expected. This is evidenced by negligible faradaic current being observed at

either the bottom (BE) or top (TE) electrodes, collected in 3-electrode configuration with external Pt counter and Ag/AgCl reference electrode, **Figure S4(a)**. When the BE and the TE were used as working and reference/counter electrode, respectively, in a 2-electrode configuration under the same solution conditions, a very small, but measurable, faradaic current due to $Fe(CN)_6^{3/4-}$ at 0 V was superimposed on the capacitive current, **Figure S4(b)**, likely resulting from a small amount of leakage.

Next, the BE was used as working electrode in a 3-elecrode configuration with external Pt counter and Ag/AgCl reference electrodes, to perform chronoamperometry with multiple potential steps ranging from –0.5 V to –2.8 V in order to stimulate mass transport through the hydrophobic P4VP nanochannels upon potential-induced wetting. As shown in **Figure 5(a)**, negligible current is observed until –2.0 V, suggesting a threshold potential to induce wetting in the hydrophobic P4VP domains of the membrane. However, when E_{BE} is increased to –2.5 V, a current bust with fluctuations is observed, consistent with the P4VP nanochannels being switched to the wetted state. The current fluctuations are similar to the stochastic fluctuations reported by others, which have been assigned to rapid dynamics reflecting the competition between condensation and evaporation of water in the hydrophobic nanochannels.[16-20, 26] At E_{BE} = –2.8 V, a second current bust is recorded with stronger fluctuations, consistent with a higher number of nanochannels participating in potential-induced wetting/dewetting.

After introducing electrolyte solution into the interior of the nanopores through these multiple potential steps, cyclic voltammetry was performed to confirm the successful introduction of electrolyte solution and its subsequent isolation from the bulk by the BCP membrane, by switching the potential back to a value less negative than the threshold potential for wetting, *i.e.,* $E_{BE} \sim -2.0$ V. **Figure S4(c)** shows a faradaic response for 50 mM $Fe(CN)_6^{3/4-}$ (together with capacitive current), but the current is much smaller than the value obtained from

a similar NEA without a BCP (*viz.* ~0.05 μA and ~0.9 μA with and without a BCP, respectively).[20, 27] The observation of a stable *i-V* characteristic after switching the membrane to positive potentials suggests that most of the hydrophobic P4VP membrane channels recovered the original dewetted state, thereby blocking egress of the redox species out of the NEA nanopores.

Finally, redox cycling current was measured using BE and TE as working and reference/counter electrode in 2-electrode configuration. Unlike the current measured in the 3-electrode configuration, **Figure S4(c)**, a significant current amplification is achieved with an enhancement factor of ~200, as shown in **Figure S4(d)**, although non-canonical current behavior is obtained in the 2-electrode configuration, especially at low ionic strength, due to the use of the Au TE as the reference electrode.[27] The difference between non-GC (3-electrode with counter and reference outside the NEA) and GC-mode (2-electrode with BE and TE as working and counter/reference) currents clearly reflects the difference between blocked transport of redox species across the BCP (3-electrode non-GC) *vs.* the facile mass transport between BE and TE in the 2-electrode GC-mode configuration. When redox cycling (GC-mode) current was measured in a 4-electrode system, with E_{BE} being swept from +0.3 V to –0.4 V while holding E_{TE} at +0.3 V, a ~440-fold current amplification was achieved compared to the non-GC current, **Figure 5(b)**. Taken together, the significant difference in current between GC and non-GC mode clearly establishes the efficient isolation and confinement of electrolyte solution in the NEA nanopores utilizing potential-induced control of mass transport across the hydrophobic BCP membrane of a BCP@NEA structure, a control concept that we attribute to wetting/dewetting phenomena inside the membrane channels.

Conclusions

The mass transport behavior in PS-*b*-P4VP BCP membranes has been characterized as a

function of pH and applied potential in order to develop a controlled transport system, using both BCP on planar Au electrodes and BCP@NEA structures. The dominant features established are: (1) anion-selective transport at pH < pK_a(P4VP), (2a) negligible mass transport at pH > pK_a(P4VP) with no applied potential, and (2b) charge-independent mass transport at pH > pK_a(P4VP) at sufficiently negative applied potentials. These effects are consistent with potential-dependent wetting and dewetting of the membrane channels, as proposed by others.[16-20, 26] Cyclic voltammetry performed on BCP membrane-coated Au electrodes demonstrates the pH-responsive, anion-permselectivity of the BCP membranes and potential-controlled on/off mass transport switching. Solutions with pH > pK_a(P4VP) confirm that P4VP domains exist in a charge-neutral, collapsed, and hydrophobic state, which basically stays in the dewetted state, blocking transport of aqueous solution in the absence of external stimuli such as applied potentials. However, the P4VP membrane channels can be reversibly switched between the dewetted and wetted states by changing the applied potential between values positive and negative values of the threshold potential, respectively. The threshold values at which these phenomena occur are dependent on the environment, as shown by the ionic strength dependence. Furthermore, BCP@NEA structures have been employed to demonstrate intelligent sampling operations. The sequence used here consists of (*a*) negative potential-induced opening of the PS-*b*-P4VP BCP membrane channels, which (*b*) enables transport of redox active probe species into the NEA nanopores, followed by (*c*) switching the applied potential back to a positive value or releasing the applied potential, rendering the membrane channels back to a dewetted state, which then (*d*) traps the probe species in the NEA nanopore. Importantly, these manipulations of the transport of electrolyte solution are achieved at pH > pK_a(P4VP), conditions under which no transport occurs in the absence of applied potential, and are thus attributed to reversible switching between wetted and dewetted states of the P4VP membrane channels.

The next phase of this research will be aimed at practical sensing applications, especially the use of these structures to achieve signal amplification from nanoconfined enzymes. In conventional electrochemical sensors, the catalytic products of enzymes immobilized on electrode surfaces can diffuse away from the electrode, diminishing the magnitude of the signal from the enzymatic products by reducing their effective concentration. By confining enzyme products in nanopores, the small volumes can support ultrasensitive sensing by accumulating enzyme products over time and generating an amplified current. Additionally, intelligent mass transport control enabled by the PS-*b*-P4VP BCP membrane may also be useful in single-molecule studies, where long residence times are required to monitor reaction dynamics as well as static and dynamic heterogeneity.

Experimental Section

Chemicals and Materials. Potassium nitrate (KNO_3), potassium ferricyanide(III) ($K_3Fe(CN)_6$), potassium ferrocyanide(II) ($K_4Fe(CN)_6$), and hexaammineruthenium(III) chloride ($Ru(NH_3)_6Cl_3$) were purchased from Sigma-Aldrich. Polystyrene-*b*-poly(4-vinyl pyridine) (PS_{48400}-*b*-$P4VP_{21300}$ M_w/M_n = 1.09) was obtained from Polymer Source Inc.. Poly(dimethylsiloxane) (PDMS) monomer and curing agent were purchased from Dow Corning. All electrolyte solutions were prepared using deionized (DI) water for electrochemical measurements ($\rho \sim 18.2$ MΩ cm, Millipore Milli-Q system). Gold electrodes were prepared by depositing 100 nm Au (UNIVEX 450B, Oerlikon) on pre-cleaned glass slides (Glass D, Applied Microarrays, Inc.)

Preparation of BCP membranes. Approximately 200 μL of a solution 2–3% (w/v) PS-*b*-P4VP in dioxane was drop cast onto a Au electrode (or a Si wafer) and then immediately

spin-coated at various speed (*typ*. 500–6000 rpm for 1 min). As-spun BCP membranes were immersed in ethanol for 30 min then dried with N_2. To transfer BCP membranes from a silicon carrier onto an NEA device, thermal release tape was first attached to the BCP membrane. When immersed in water, the BCP membrane was detached from the Si wafer, and remaining moisture on the BCP membrane was removed by N_2. Then the BCP membrane was attached to the NEA surface, taking care to avoid trapping air at the interface. In the final step, the BCP membrane-coated NEA was placed on a hot plate heated at 100 °C to spontaneously detach the thermal release tape from the BCP.

Fabrication and characterization of BCP@NEA membranes. NEAs were fabricated by following the previous methods reported elsewhere by this laboratory, except that in these experiments a much thicker layer of SiO_2 (500 nm) was used.[27-29] The BCP@NEA structures were characterized using scanning electron microscopy (FEI-Helios Dual-beam focused ion beam). In order to minimize charging effects, 5 nm Ir was deposited onto the BCP membrane prior to SEM imaging. Typically, an accelerating voltage of 5 kV and an electron beam current of 0.1 nA were used for clear structural observation of the BCP@NEA.

Electrochemical measurements. In order to perform electrochemical measurements, a PDMS well with 6 mm diameter was constructed on BCP-coated Au electrode and then filled with *ca*. 100 μL electrolyte solution. Cyclic voltammetry (CV) and multiple potential step experiments were conducted in 3-electrode system with a Pt wire counter electrode and a Ag/AgCl reference electrode (Harvard Apparatus, USA) using either CHI842C or CHI760A electrochemical workstation (CH Instruments, USA). All voltammograms were obtained with a scan rate of 100 mV s^{-1}. For current-time measurements with multiple potential steps, current sampling frequency was set at 5 kHz to faithfully trace transient changes in current.

Author contributions

S.-R. Kwon contributed to NEA device fabrication, BCP@NEA construction, electrochemical measurements, and analysis. S. Baek conducted BCP membrane preparation, SEM image analysis, electrochemical measurements, and analysis. P. W. Bohn contributed to planning experiments and analyzing data. All authors participated in scientific discussion for data analysis, and writing/revising of the manuscript.

Conflicts of interest

There are no conflicts to declare.

Acknowledgements

The development of the BCP@NEA structures was supported by the National Science Foundation through grant 1904196, and the wetting/dewetting experiments were supported by the Department of Energy Office of Science through grant DE FG02 07ER15851. The authors gratefully acknowledge Notre Dame Nanofabrication Facility and Integrated Imaging Facility for providing fabrication and characterization support.

Author information

Corresponding Author

*E-mail: pbohn@nd.edu. Tel.: +1 574 631 1849. Fax: +1 574 631 8366.

ORCID

Seung-Ryong Kwon: 0000-0002-0890-523X

Seol Baek: 0000-0003-2191-6723

Paul W. Bohn: 0000-0001-9052-0349

Additional information

Supporting Information: Supporting Information is available free of charge.

References

1. D. A. Doyle, J. M. Cabral, R. A. Pfuetzner, A. Kuo, J. M. Gulbis, S. L. Cohen, B. T. Chait and R. MacKinnon, *Science*, 1998, **280**, 69-77.
2. E. Gouaux and R. MacKinnon, *Science*, 2005, **310**, 1461-1465.
3. O. Beckstein and M. S. P. Sansom, *Phys. Biol.*, 2006, **3**, 147-159.
4. M. Ø. Jensen, D. W. Borhani, K. Lindorff-Larsen, P. Maragakis, V. Jogini, M. P. Eastwood, R. O. Dror and D. E. Shaw, *Proc. Natl. Acad. Sci. U. S. A.*, 2010, **107**, 5833-5838.
5. C. Neale, N. Chakrabarti, P. Pomorski, E. F. Pai and R. Pomès, *PLoS Comput. Biol.*, 2015, **11**, e1004303.
6. S. Balme, F. Picaud, M. Manghi, J. Palmeri, M. Bechelany, S. Cabello-Aguilar, A. Abou-Chaaya, P. Miele, E. Balanzat and J. M. Janot, *Sci. Rep.*, 2015, **5**, 10135.
7. L. Chen, W. Wang, B. Su, Y. Wen, C. Li, Y. Zhou, M. Li, X. Shi, H. Du, Y. Song and L. Jiang, *ACS Nano*, 2014, **8**, 744-751.
8. Q. Zhang, J. Kang, Z. Xie, X. Diao, Z. Liu and J. Zhai, *Adv. Mater.*, 2018, **30**, 1703323.
9. Y. Cheng, X. Jiao, L. Zhao, Y. Liu, F. Wang, Y. Wen and X. Zhang, *J. Mater. Chem. B*, 2018, **6**, 6269-6277.
10. Z. Zhang, X.-Y. Kong, K. Xiao, Q. Liu, G. Xie, P. Li, J. Ma, Y. Tian, L. Wen and L. Jiang, *J. Am. Chem. Soc.*, 2015, **137**, 14765-14772.
11. E. D. Steinle, D. T. Mitchell, M. Wirtz, S. B. Lee, V. Y. Young and C. R. Martin, *Anal. Chem.*, 2002, **74**, 2416-2422.
12. G. Pérez-Mitta, A. G. Albesa, C. Trautmann, M. E. Toimil-Molares and O. Azzaroni, *Chemical Science*, 2017, **8**, 890-913.
13. I. Vlassiouk, C.-D. Park, S. A. Vail, D. Gust and S. Smirnov, *Nano Lett.*, 2006, **6**, 1013-1017.

14. F. Rios and S. N. Smirnov, *Chem. Mater.*, 2011, **23**, 3601-3605.

15. S. Smirnov, I. Vlassiouk, P. Takmakov and F. Rios, *ACS Nano*, 2010, **4**, 5069-5075.

16. S. N. Smirnov, I. V. Vlassiouk and N. V. Lavrik, *ACS Nano*, 2011, **5**, 7453-7461.

17. M. R. Powell, L. Cleary, M. Davenport, K. J. Shea and Z. S. Siwy, *Nat. Nanotechnol.*, 2011, **6**, 798-802.

18. K. Xiao, Y. Zhou, X.-Y. Kong, G. Xie, P. Li, Z. Zhang, L. Wen and L. Jiang, *ACS Nano*, 2016, **10**, 9703-9709.

19. G. Xie, P. Li, Z. Zhao, Z. Zhu, X.-Y. Kong, Z. Zhang, K. Xiao, L. Wen and L. Jiang, *J. Am. Chem. Soc.*, 2018, **140**, 4552-4559.

20. S.-R. Kwon, S. Baek, K. Fu and P. W. Bohn, *Small*, 2020, **16**, 1907249.

21. C. Ma, N. M. Contento and P. W. Bohn, *J. Am. Chem. Soc.*, 2014, **136**, 7225-7228.

22. K. Fu and P. W. Bohn, *ACS Appl. Mater. Interfaces*, 2017, **9**, 24908-24916.

23. K. Fu, D. Han, S.-R. Kwon and P. W. Bohn, *ACS Nano*, 2018, **12**, 9177-9185.

24. S. Baek, S.-R. Kwon, K. Fu and P. W. Bohn, *ACS Appl. Mater. Interfaces*, 2020, **12**, 55116-55124.

25. Y. Wu, K. Wang, H. Tan, J. Xu and J. Zhu, *Langmuir*, 2017, **33**, 9889-9896.

26. L. Innes, D. Gutierrez, W. Mann, S. F. Buchsbaum and Z. S. Siwy, *Analyst*, 2015, **140**, 4804-4812.

27. S.-R. Kwon, K. Fu, D. Han and P. W. Bohn, *ACS Nano*, 2018, **12**, 12923-12931.

28. K. Fu, D. Han, C. Ma and P. W. Bohn, *Nanoscale*, 2017, **9**, 5164-5171.

29. K. Fu, D. Han, C. Ma and P. W. Bohn, *Faraday Discuss.*, 2016, **193**, 51-64.

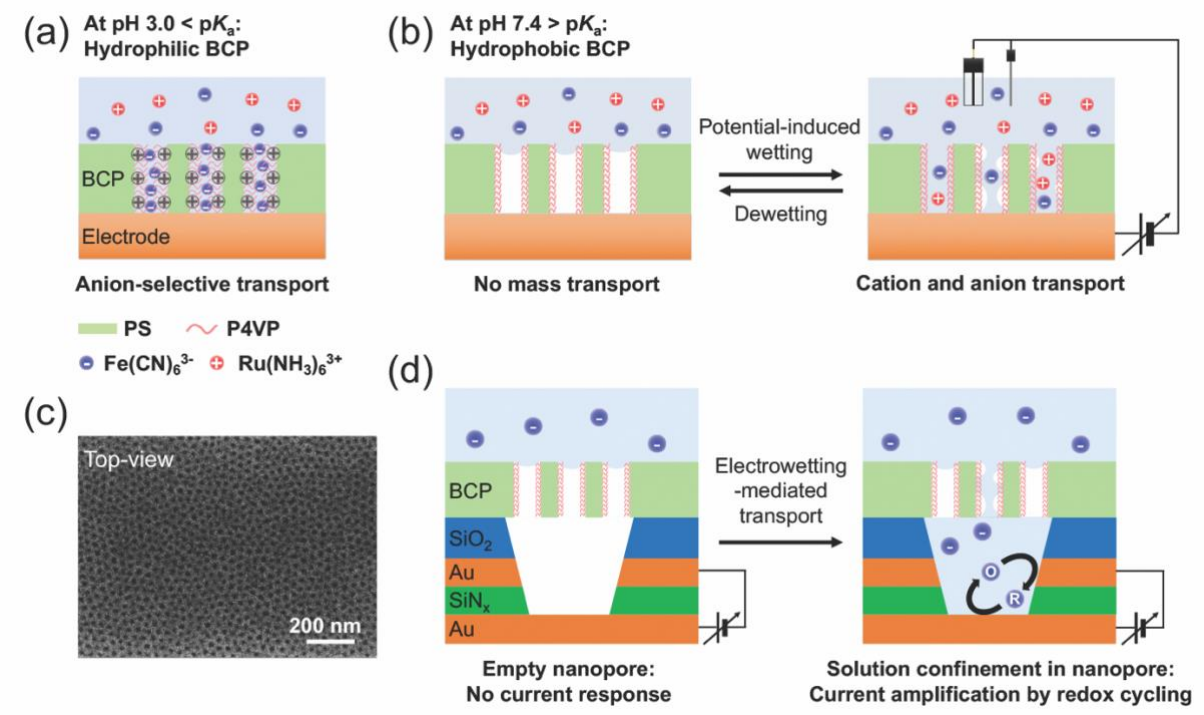

Figure 1. Schematic illustration of the PS-*b*-P4VP BCP membrane showing 3 types of mass transport actions controlled by pH and potential. (a) Anion-selective transport at pH < pK_a(P4VP). (b) On/off mass transport switching between no transport (*left*) and charge-independent transport controlled by applied potential (*right*) at pH > pK_a(P4VP). (c) Top-view SEM image of the BCP membrane spun onto a planar Au electrode showing hexagonally packed cylindrical domains of P4VP. (d) Schematic illustration of a BCP@NEA structure at pH > pK_a(P4VP). Mass transport into the nanopore is initially blocked by the hydrophobic character of the membrane (*left*). It may be temporarily opened for mass transport across the membrane by electric-field-induced wetting of the P4VP nanochannels, resulting in nanopore-filling and subsequent redox cycling-based current amplification using BE and TE as working- and counter-electrodes, respectively (*right*).

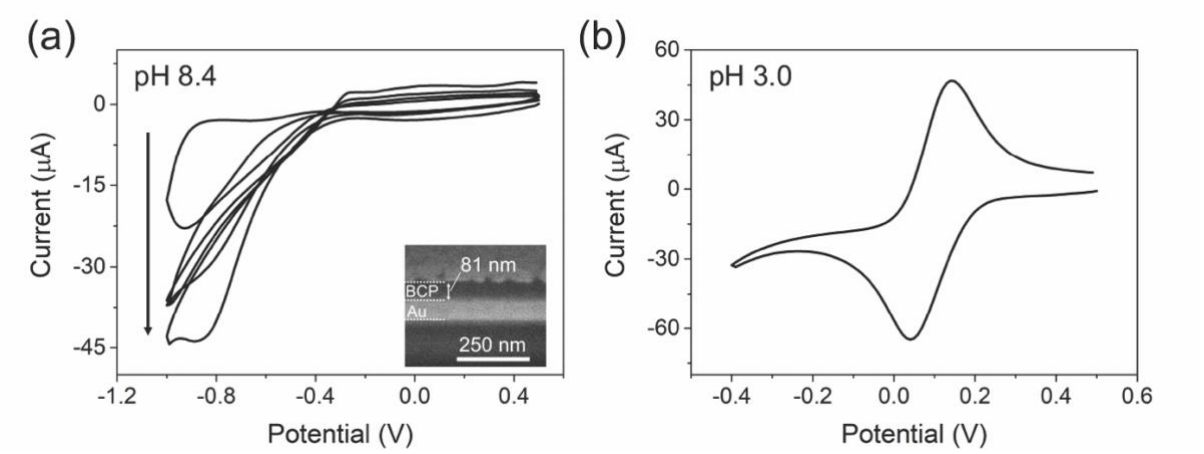

Figure 2. Voltammograms of 5 mM $Fe(CN)_6^{3-}$ in 0.1 M KCl at pH 8.4 (a) and 3.0 (b) on BCP-coated planar Au electrode. Arrow indicates direction of increasing scan numbers. The cross-sectional SEM image in panel (a) shows the thickness of the BCP membrane on the Au electrode obtained by spin-coating at 6000 rpm for 1 min.

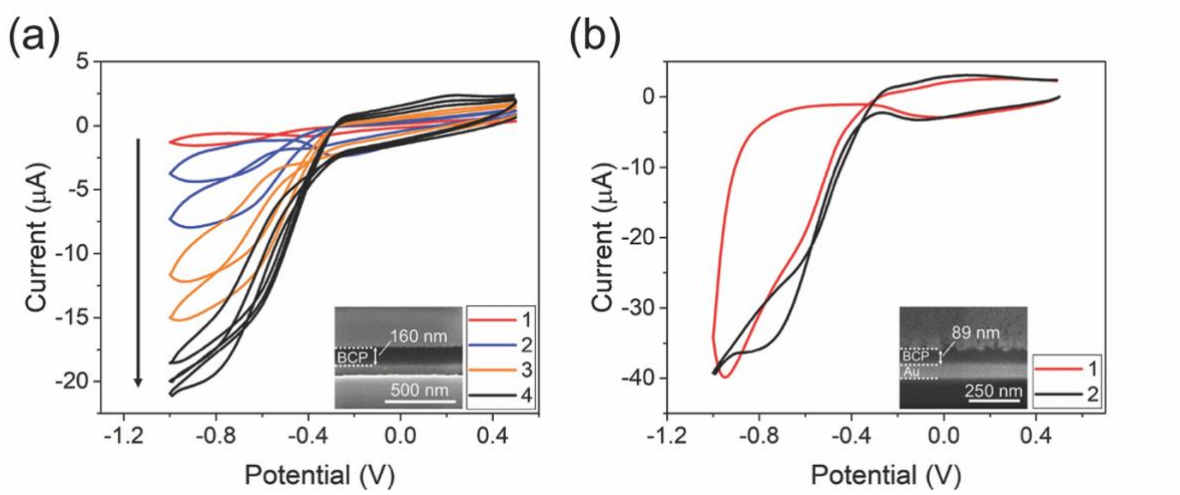

Figure 3. Voltammograms of 5 mM $Ru(NH_3)_6^{3+}$ in 0.1 M KCl at pH 7.8 on (a) 160 nm thick and (b) 89 nm thick BCP membranes on Au. The arrow in panel (a) indicates increasing scan numbers. Insets show cross-sectional SEM images of the BCP membranes spin-coated on Au.

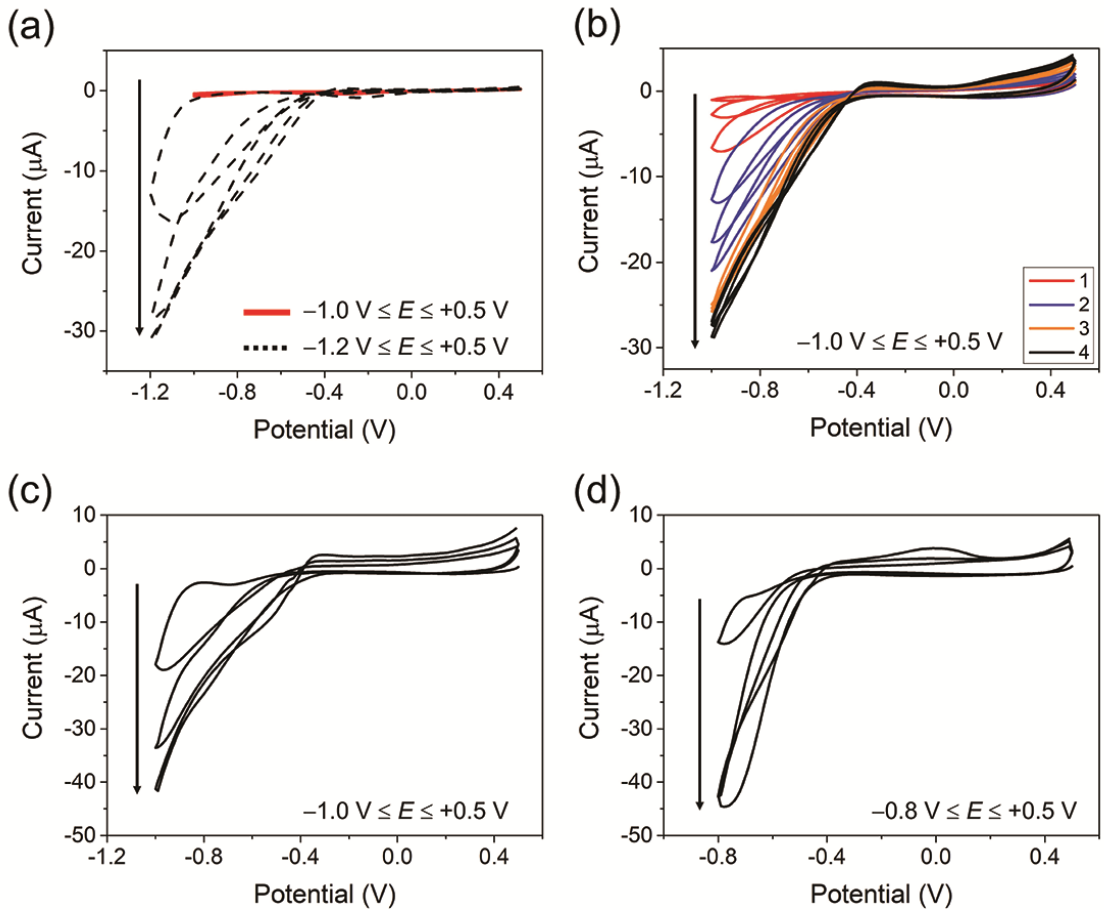

Figure 4. Voltammetric responses of 1 mM $Fe(CN)_6^{3-}$ at varying concentration of supporting electrolyte: (a) 0 mM; (b) 10 mM; (c) 100 mM; and (d) 1000 mM KNO_3.

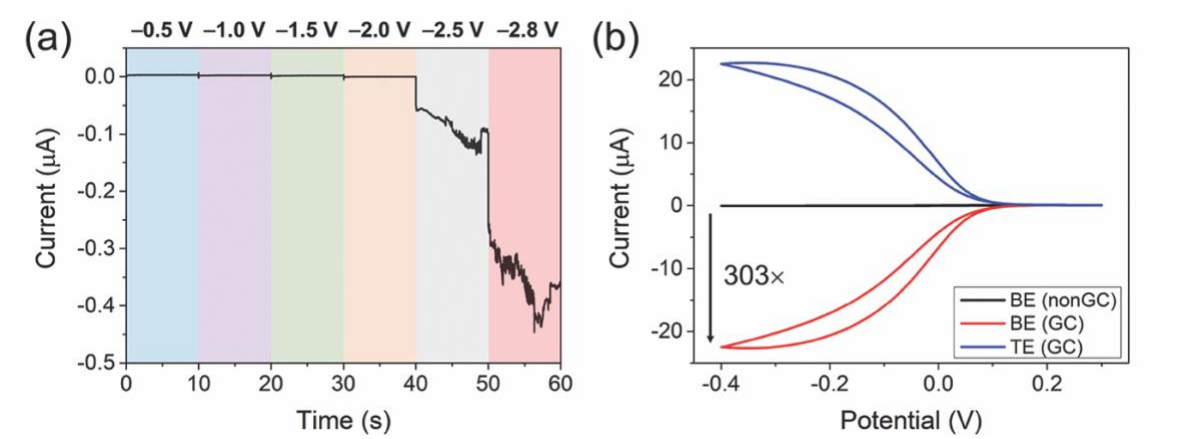

Figure 5. (a) Chronoamperometric response of 50 mM $Fe(CN)_6^{3/4-}$ with no supporting electrolyte at pH 7.6 to multiple potential steps at a BCP@NEA structure. BE was used as working electrode, with E_{BE} = –0.5 V, –1.0 V, –1.5 V, –2.0 V, –2.5 V, and –2.8 V, in a 3-electrode configuration with external Pt wire counter and Ag/AgCl reference electrode. Current sampling frequency was set at 5 kHz. (b) Voltammograms measured in generator-collector (GC) mode and non-GC mode on a BCP@NEA structure. For GC mode operation, E_{BE} was swept from +0.3 V to –0.4 V while E_{TE} was held at +0.3 V in the 4-electrode configuration with Pt counter and Ag/AgCl reference electrode. Non-GC mode current was obtained with BE in the 3-electrode configuration with E_{TE} left at open-circuit potential.

Supporting Information for

Potential-Induced Wetting and Dewetting in pH-Responsive Block Copolymer Membranes for Mass Transport Control

Seung-Ryong Kwon[1†], Seol Baek[2†], and Paul W. Bohn[2,3*]

[1]Department of Chemistry and Research Institute of Natural Science, Gyeongsang National University, Jinju, 52828, South Korea

[2]Department of Chemistry and Biochemistry, University of Notre Dame, Notre Dame, Indiana 46556, United States

[3]Department of Chemical and Biomolecular Engineering, University of Notre Dame, Notre Dame, Indiana 46556, United States

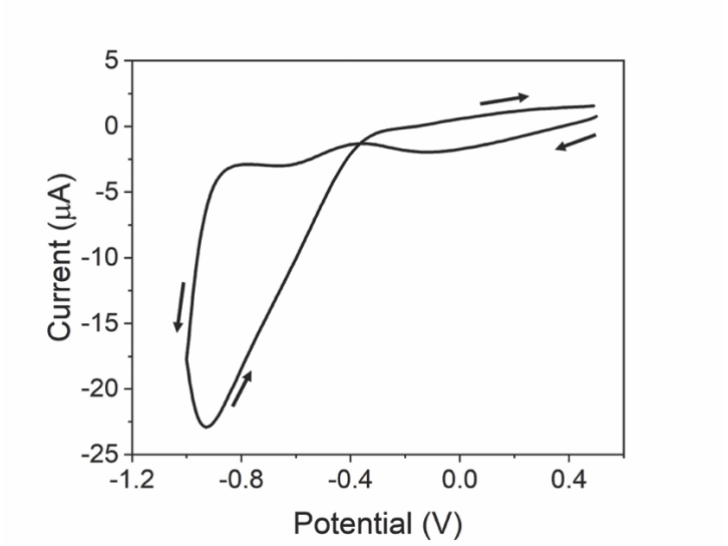

Figure S1. Voltammetric response of 5 mM $Fe(CN)_6^{3-}$ in 0.1 M KCl on a BCP-coated Au electrode at pH 8.4 showing only the first potential scan in panel (a) of **Figure 2**.

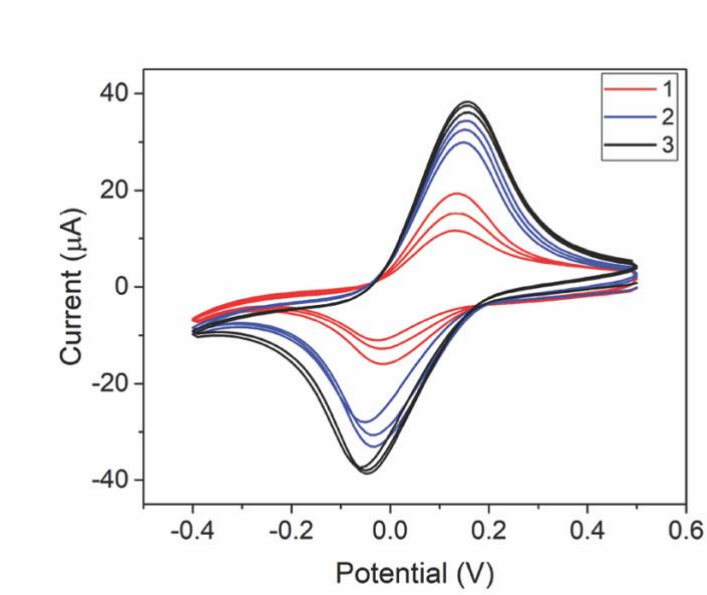

Figure S2. Consecutive voltammograms of 1 mM $Fe(CN)_6^{3-}$ in 0 mM KNO_3 at pH 3.1 on BCP-coated Au electrode after switching electrolyte solution from pH 8.4. The numbers indicate the order in which the voltammograms were obtained. Each voltametric set consists of 3 potential cycles.

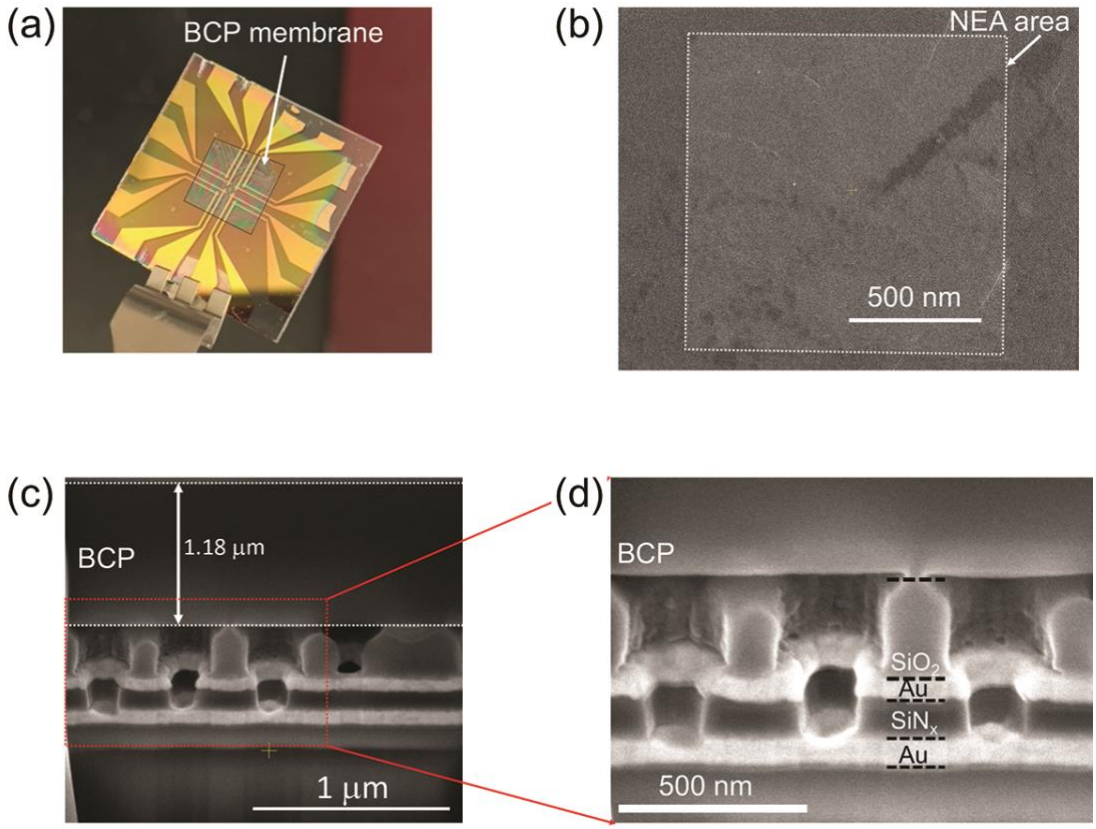

Figure S3. (a) Photographic image of a BCP@NEA device. (b) Top view SEM image of the BCP membrane-coated NEA. (c,d) Cross-sectional SEM images revealing membrane thickness (c) and the detailed nanopore structures beneath the BCP membrane (d). The physical integrity of the nanopores in contact with the BCP membranes is apparent from these images.

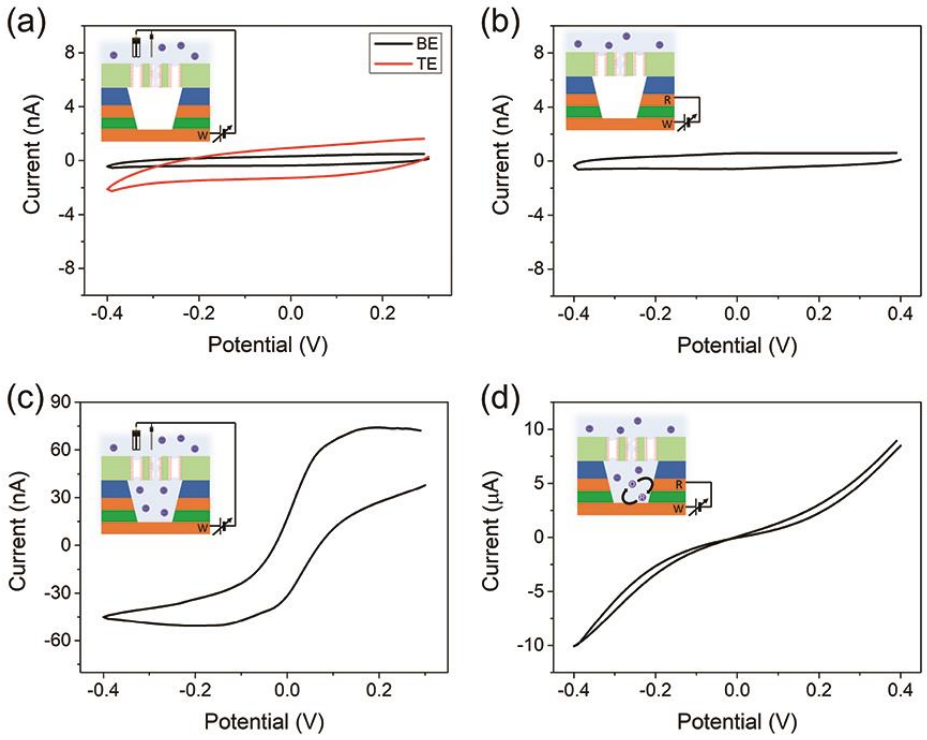

Figure S4. (a,c) Non-GC mode and (b,d) GC mode voltametric responses of 50 mM $Fe(CN)_6^{3/4-}$ in no SE at pH 7.6 in the 3-electrode (a,c) and 2-electrode (b,d) configurations. Voltammetric responses were obtained in the presence of the BCP membrane before (a,b) and after (c,d) potential-induced solution introduction into the nanopores. Non-GC current was obtained either with BE or TE in the 3-electrode configuration with a Pt wire counter and Ag/AgCl reference electrode, situated outside the NEAs. GC operation was conducted in a 2-electrode configuration, where BE and TE were used as working and reference/counter electrodes, respectively.